International Journal of Applied Earth Observation and Geoinformation 54 (2017) 72–83

Contents lists available at ScienceDirect

International Journal of Applied Earth Observation and Geoinformation

journal homepage: www.elsevier.com/locate/jag

Phenology from Landsat when data is scarce: Using MODIS and Dynamic Time-Warping to combine multi-year Landsat imagery to derive annual phenology curves

Matthias Baumann[a,*], Mutlu Ozdogan[b], Andrew D. Richardson[c], Volker C. Radeloff[d]

[a] Geography Department, Humboldt-University Berlin, Unter den Linden 6, 10099 Berlin, Germany
[b] Department of Forest and Wildlife Ecology, University of Wisconsin-Madison, 1630 Linden Drive, Madison, WI 53706, USA
[c] Department of Organismic and Evolutionary Biology, Harvard University, 22 Divinity Avenue, Cambridge, MA 021038, USA
[d] SILVIS Lab, Department of Forest and Wildlife Ecology, University of Wisconsin-Madison, 1630 Linden Drive, Madison, WI 53706, USA

ARTICLE INFO

Article history:
Received 11 January 2016
Received in revised form 31 August 2016
Accepted 9 September 2016
Available online 16 September 2016

Keywords:
Landsat
Dynamic time warping
Green-leaf phenology
PhenoCam
MODIS
EVI

ABSTRACT

Green-leaf phenology describes the development of vegetation throughout a growing season and greatly affects the interaction between climate and the biosphere. Remote sensing is a valuable tool to characterize phenology over large areas but doing at fine- to medium resolution (e.g., with Landsat data) is difficult because of low numbers of cloud-free images in a single year. One way to overcome data availability limitations is to merge multi-year imagery into one time series, but this requires accounting for phenological differences among years. Here we present a new approach that employed a time series of a MODIS vegetation index data to quantify interannual differences in phenology, and Dynamic Time Warping (DTW) to re-align multi-year Landsat images to a common phenology that eliminates year-to-year phenological differences. This allowed us to estimate annual phenology curves from Landsat between 2002 and 2012 from which we extracted key phenological dates in a Monte-Carlo simulation design, including green-up (GU), start-of-season (SoS), maturity (Mat), senescence (Sen), end-of-season (EoS) and dormancy (Dorm). We tested our approach in eight locations across the United States that represented forests of different types and without signs of recent forest disturbance. We compared Landsat-based phenological transition dates to those derived from MODIS and ground-based camera data from the PhenoCam-network. The Landsat and MODIS comparison showed strong agreement. Dates of green-up, start-of-season and maturity were highly correlated (r 0.86-0.95), as were senescence and end-of-season dates ($r > 0.85$) and dormancy ($r > 0.75$). Agreement between the Landsat and PhenoCam was generally lower, but correlation coefficients still exceeded 0.8 for all dates. In addition, because of the high data density in the new Landsat time series, the confidence intervals of the estimated keydates were substantially lower than in case of MODIS and PhenoCam. Our study thus suggests that by exploiting multi-year Landsat imagery and calibrating it with MODIS data it is possible to describe green-leaf phenology at much finer spatial resolution than previously possible, highlighting the potential for fine scale phenology maps using the rich Landsat data archive over large areas.

1. Introduction

Green-leaf phenology is an important attribute of vegetation throughout the growing season and key for quantifying the water, energy, and carbon exchange between atmosphere and biosphere (Wolfe et al., 2005; Zhang et al., 2006; Richardson et al., 2013). Satellite data can capture green-leaf phenology across large areas due to their standardized and repeated measurements (Asner et al., 2000; Knudby 2004; Paruelo et al., 1997; Roetzer et al., 2000; Tucker et al., 1986). For example, Moderate Resolution Image Spectroradiometer (MODIS) data characterize green-leaf phenology across the globe in a standard MODIS product (Ganguly et al., 2010; Zhang et al., 2006, 2003). For many applications, such as the estimation of ecosystem net primary production (Goward et al., 1985) and annual evapotranspiration (Sun et al., 2004) over large areas, the spatial resolution of MODIS phenology data (250–500 m) is well suited. However, green-leaf phenology is also important for ecological processes that operate at much finer spatial scales such as the characterization of stop-over sites for migratory birds (Wood and Pidgeon 2015; Wood et al., 2012), or habitat selection by deer

* Corresponding author.
E-mail address: matthias.baumann@geo.hu-berlin.de (M. Baumann).

http://dx.doi.org/10.1016/j.jag.2016.09.005
0303-2434/

(Schaefer et al., 2008) or badgers (Santos et al., 2014; Schaefer et al., 2008). Likewise, the mapping of tree species in heterogeneous forest landscapes can be greatly enhanced with green-leaf phenology data (Wolter et al., 1995; Wolter and Townsend 2011) because the timing of green-up in the spring and senescence in the fall varies substantially among different species (Lechowicz 1984; Richardson et al., 2006), and also within the same species due to environmental variation (Crawley and Akhteruzzaman, 1988; Luquez et al., 2008). Indeed, even genetic differences within the same species, e.g. aspen (*Populus tremula*), can influence the timing of the green-up in spring (Hall et al., 2007; Li et al., 2010). However, the resolution of MODIS data does not suffice to capture such fine-scale differences in phenology, and green-leaf phenology derived from medium-resolution satellite data would be valuable for many ecological applications.

Landsat satellites provide images with medium spatial resolution (30 m) and provide thanks to over 40 years of continuous observations an unprecedented archive of the Earth's terrestrial landscape (Loveland and Dwyer, 2012). Landsat satellites have been used to describe vegetation phenology since the early years of Landsat Multispectral Scanner (MSS) for assessments of canopy composition (Tucker, 1979). With their higher spatial resolution, multi-temporal imagery of Landsat Thematic Mapper (TM) provided the basis for capturing vegetation at different phenological stages ultimately allowing to discriminate between different tree types in the US-Northeast (Schriever and Congalton, 1995) and the Midwest (Wolter et al., 1995). However, the low temporal resolution of Landsat data and frequent cloud obstructions have limited the use of Landsat data for tree species mapping because the number of cloud-free images in a given year is often low.

In recent years, free and open access to the Landsat archive has triggered a proliferation of new methods and products in phenological research using both Landsat TM and Enhanced Thematic Plus (ETM+) data (Wulder et al., 2012). For example, dense time-series of Web Enabled Landsat Data (WELD) helped deriving agricultural field boundaries based on the phenological characteristics of crops over a year (Yan and Roy, 2014), and to relate Landsat phenology observations to observations from flux tower measurements (Kovalskyy et al., 2011). Likewise, multi-year Landsat observations over New England (USA) merged into a single time series, revealed that spring onset dates of homogenous deciduous forest stands exhibit substantial local variability (Fisher et al., 2006), and that the start and end of the growing season varied by as much as four weeks over a thirty-year time period (Melaas et al., 2013).

However, some of these studies also highlight the low temporal availability of Landsat data as a major limitation for phenology studies, probably due to archive consolidation issues, scan-line corrector failure (SLC-off), or excessive cloud coverage. To overcome this issue, two primary pathways have been suggested in the literature. On one hand, Landsat data can be fused with data from a satellite of higher temporal resolution (e.g., MODIS) in order to model Landsat-like images, thereby creating a high-temporal, cloud-free time series (Gao et al., 2006; Hilker et al., 2009) that characterizes phenology (Bhandari et al., 2012; Walker et al., 2014, 2012). On the other hand, Landsat images from multiple years can be merged into a single time series (Melaas et al., 2013). In this case, however, the multi-year observations need to be adjusted in order to account for inter-annual differences in phenology. This can be done in several different ways. For example, through the introduction of a time lag factor within the phenology model, one can calculate a phase-shift and adjust the timing of each observation according to the global mean of all observations (Fisher et al., 2006). The downside of this approach, however, is that the modelled phenology is attributed to an 'average' year rather than to a specific year, preventing the analysis of trends in phenology over multiple years.

Alternatively, one can use a dense time series from a different sensor in conjunction with Landsat data to account for phenological differences among years. Observations from this sensor may be of coarser spatial resolution, as long as they have sufficient temporal resolution to capture phenology well, thereby providing a 'reference phenology'. Using this reference phenology, multi-year Landsat observations can then be re-ordered based on a rule-set, for example the 'days left in season' (Isaacson et al., 2012). However, this approach is limited to observations during the second half of the growing season, and does not apply to observations during spring and summer. Given the ecological importance of the start of season and other phenological metrics, it would be desirable to develop an approach that makes use of all observations through a given year under the reference phenology framework.

Dynamic Time Warping (DTW) is a promising algorithm designed to generate a ruleset based on a complementary dataset. DTW, originally developed for speech recognition (Sakoe and Chiba, 1978), has increasingly been used in remote sensing applications, for example for detection of sugar cane fields (Romani et al., 2010), image clustering (Weber et al., 2012), re-ordering irregularly distributed time series (Petitjean et al., 2012, 2011) and, in at least one case, to estimate phenology (Huseby et al., 2005). The basic idea of DTW is that while two time series may follow a trajectory that generally makes them very similar to each other, for a given date these time series may vary substantially. For example, the phenological cycle of forest canopies, manifested by the green-up, maturity, and the senescence stages may display some temporal variation among years due to weather conditions. However, there will always be a green-up phase in tree canopies followed by maturity, and senescence. In other words, in each year, the phenological trajectory will follow a curve reminiscent of a double logistic function, but the parameters of the function will vary from year to year (Huseby et al., 2005). We propose that DTW may be applicable for our purpose of accounting for the differences among the phenologies of different years to create a ruleset that allows re-ordering Landsat imagery from a multi-year time series. Here, we used MODIS phenology curves to create such a ruleset for re-ordering Landsat imagery from 2002 to 2012. Based on this very dense Landsat time series, we then modelled a Landsat phenology curve for each individual target year.

Generating a new dataset inevitably raises questions regarding its accuracy, and how to validate it. A comparison of the resulting Landsat phenology curve with the MODIS phenology curve alone would be somewhat circular, because the MODIS phenology curve was already used to generate the new Landsat phenology curve. However, data from the PhenoCam network provides an independent assessment of phenology. PhenoCam data monitor seasonal development of vegetation on the ground at a very high temporal resolution (Richardson et al., 2009), and can be linked to remotely sensed estimates of phenology (Klostermann et al., 2014) such as the timing of spring and autumn, and growing season length (Elmore et al., 2012; Hufkens et al., 2012; Keenan et al., 2014). Here, we compared the new Landsat phenology curve to the ground-based PhenoCam phenology curve, as well as to the MODIS phenology curve in regards to multiple different phenological 'key dates' (e.g., green-up, maturity, etc.) that describe the development, maturity, and the senescence of natural vegetation canopies.

Our overarching goal was to assess phenology from Landsat data, where data availability is limited, by generating a phenology product that characterizes the phenological evolution for each year between 2002 and 2012 and that is comparable to the MODIS phenology. Specifically, our objectives were to:

1. use MODIS EVI time series and DTW to derive a ruleset that relates the phenology of different years to each other, and apply

Table 1
Study sites and datasets, used in the study. Years indicate the years with complete phenology in the PhenoCam-data.

Study Site Name	Lat	Long	Years	Landsat Path/Row	MODIS tile	Characterization
Arbutus Lake	43.98	−74.23	2009, 2010, 2012	015/029	h12 v04	Mostly deciduous, in background more coniferous, only little understory
Bartlett	44.06	−71.29	2008, 2009, 2011, 2012	012/029	h12 v04	Mixed forest, deciduous species dominant, some understory
Cary Institute	41.78	−73.73	2010–2012	014/031	h12 v04	Mostly deciduous, view from side, amount of understory unclear
Harvard Forest	42.54	−72.17	2009–2012	013/030	h12 v04	Mostly deciduous, some coniferous, understory present
Mammoth Cave	37.18	−86.10	2003–2012	021/034	h11 v05	Deciduous forest, amount of understory unclear
Morgan Monroe State Forest	39.32	−86.41	2003–2009 2011–2012	021/033	h11 v05	Dominant deciduous, little understory
Univ. Michigan Biological Station	45.55	−84.71	2010–2012	021/028	h12 v04	Mostly deciduous, some coniferous in the foreground, understory

the rule-set to all available Landsat imagery to generate a Landsat phenology curve for each year between 2002 and 2012,
2. calculate a set of phenological key dates and assess the trend of the key dates from a time series of Landsat phenologies between 2002 and 2012, and
3. compare the generated Landsat phenology to a phenology from PhenoCam digital camera time series and the MODIS phenology based on the phenological 'key dates'.

2. Methods

2.1. Dynamic Time Warping and generation of a Landsat phenology curve

For this study, we define 'phenology curve' as the fitted curve through a time series of Enhanced Vegetation Index (EVI) values of one year. We used DTW to align the phenology curve of one year (i.e., the query phenology) to the phenology curve of a second year (i.e., the target phenology). In general, DTW takes the query phenology curve and stretches and compresses it to make it as similar as possible to the target phenology curve (Giorgino 2009; Petitjean et al., 2011), resulting in a ruleset of phenologically corresponding days, which we applied to a dense time series of multi-year Landsat imagery. In a first step, we generated the MODIS reference.

In a first step, we generated the MODIS reference phenology curve that described the broad-scale phenological evolution of vegetation from 2002 to 2012. To do this, we extracted the Enhanced Vegetation Index (EVI) values from a time series of 8-day MODIS 500-m EVI data from Aqua and Terra (MODIS products MOD13A1 and MYD13A1), thereby removing observations of poor quality based on the MODIS quality assessment to reduce the effects of clouds, ice, and snow. We then fitted a double logistic curve to the MODIS EVI time series for each year individually (Zhang et al., 2006, 2003). We added parameters to the double logistic function to control the phase of green-up and senescence and thereby fully capture the phenological dynamics (Elmore et al., 2012; Melaas et al., 2013). Specifically, we estimated the phenology for each year with the following Eq. (1):

$$EVI_d(t) = m_1 + (m_2 - m_7 \cdot t) \cdot \left(\frac{1}{1 + e^{((m_3 - t)/m_4)}} - \frac{1}{1 + e^{((m_5 - t)/m_6)}} \right) \quad (1)$$

where EVI_d is the EVI at each day of the year, t is the day of year, m_1 is the minimum EVI and m_2 the amplitude of EVI during the year, $m_{3,4}$ and $m_{5,6}$ are the parameters to control the phase of green-up ($m_{3,4}$) and senescence ($m_{5,6}$), and m_7 the summer green-down (Elmore et al., 2012; Fisher et al., 2006; Melaas et al., 2013). We extracted parameters m_1 and m_2 from the MODIS-EVI time series, and estimated the remaining parameters by least squares curve fitting using the Levenberg-Marquard algorithm (Moré, 1978).

In the second step, we selected a target year defined as the year to which the other years of MODIS phenologies were warped to. For example, if 2012 was chosen as the target year, the phenology curves of all other years (i.e., 2002–2011) were warped to that year. For simplicity, we reduce the following method description to the target year 2012(T^{12}) and one other year (i.e., 2011, hereafter the 'query' year (Q^{11})) which is being warped to the target year, but ultimately, this was done sequentially for each year.

To warp the query year to the target year we calculated a 365-by-365 matrix, in which each element (i, j) described the Euclidean distance between the phenological value (i.e., the EVI, Fig. 1) of two days of the time series Q_i^{11} and T_j^{12}. For example, if the value at the day of the year (DOY) 20 in the query time series was 0.21, and the value of DOY 20 in the target time series was 0.25, the value at location (20,20) in the matrix was 0.04. Based on this distance matrix,

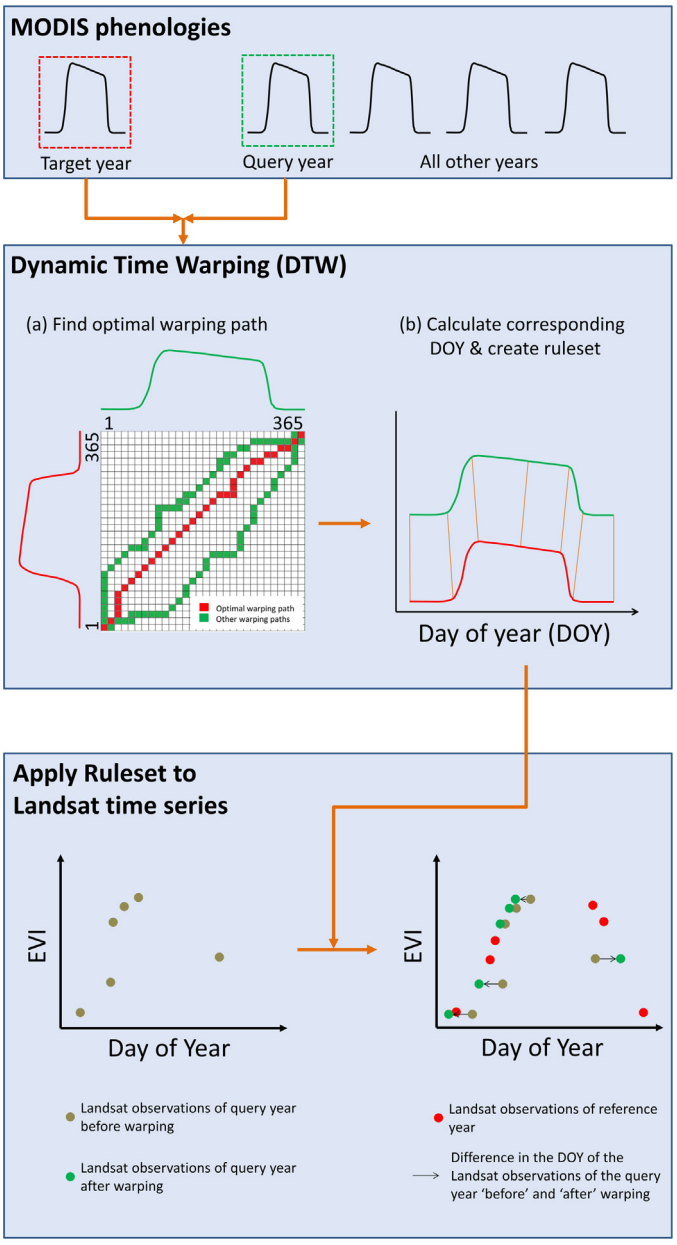

Fig. 1. Conceptual overview of the application of Dynamic Time Warping (DTW) to generate a dense Landsat time series using imagery from multiple years. Top box: selection of the phenologies of the reference year and one target year to enter the warping. In this conceptual representation, only one target phenology and one query phenology was selected. However, in reality, this procedure was done for each year between 2002 and 2012. Middle Box: schematic representation of using DTW to find the ruleset for re-aligning the Landsat observations from the query year. On the left side the selection of the optimal warping path vs. other candidate warping paths is represented. Each cell in the matrix represents a pair of day of years (DOYs) between the query and the reference year. For representation purposes, however, the matrix contains only a one cell representing 10 days (~30 × 30 cells). On the right side, the phenologically corresponding DOY between the target and the query year are highlighted. Again, for representation purposes only seven DOY-pairs are shown, but in reality each DOY of the query phenology has a corresponding DOY in the reference phenology. The Bottom box: application of the ruleset from DTW to the Landsat time series. The arrows indicate the change in the DOY of the Landsat imagery of the query year after the warping, now matching the time series of the reference year..

we calculated all possible warping paths $WP = (w_1, w_2, \ldots, w_k)$ as the sum of the matrix elements. A warping path was the combination of a number of elements in the matrix between the lower left and the upper right corner (Fig. 1).

The theoretical number of possible warping paths through the matrix is exponentially high, and in the vast majority of cases a warping path is not meaningful in the context of phenology. We therefore defined three restrictions: (a) the warping path had to start at $w_1 = (1, 1)$ and end at $w_k = (365, 365)$ and find for every DOY in Q^{11} a corresponding DOY in T^{12}, (b) the elements of a warping path had to be adjacent to another element of the matrix (continuity), and (c) the points had to be monotonically spaced in time (monotonicity, (Giorgino 2009; Romani et al., 2010)). The optimal warping path was the path that minimized the overall path-cost (i.e., the sum of all matrix elements in that path). Once we found the optimal warping path, we extracted the index values (i,j) of the warping paths, which can be interpreted as the phenological DOY in T^{12} for each DOY in Q^{11}.

In our third step we realigned the Landsat imagery by applying the ruleset from step two. Again, for simplification we use as an example for this explanation only one query year 2011 and the target year 2012, but ultimately conducted this step for each year. Prior to the application of the ruleset, we converted each raw Landsat image into surface reflectance values using the Landsat Ecosystem Disturbance Adaptive Processing System (LEDAPS (Masek et al., 2006)) and calculated the EVI. Clouds and cloud shadows were masked using Fmask (Zhu and Woodcock, 2012). We then created the new Landsat time series for the target year (i.e., 2012). Thereby, all Landsat imagery from the target year 2012 were considered in their original form, meaning that they retained their original acquisition date. The date of the Landsat imagery from the query year 2011 (i.e., their DOY in the new Landsat time series), however, was determined by the generated ruleset (Fig. 1). This yielded a dense time series of Landsat imagery representing the target year 2012, and this step was repeated until all imagery from all years was included. The result of this procedure was thus the conversion of the Landsat time series from a chronological time series (i.e., ordered by the day of the year) into a phenological time series (i.e., ordered by the phenological condition of the MODIS phenology (Huseby et al., 2005)). Using this new dense time series, we then fitted the double logistic function defined in Eq. (1), applying the same parameter estimation strategy as to the MODIS data, hence generating a Landsat phenology curve for the target year.

2.2. Extraction of phenological key dates

Once the combined phenology curve was generatedwe extracted phenological key dates based on extreme points in the continuous double logistic function. One advantage of a continuous function is that it allows for the automated extraction of such extreme points based on the curvature rates, which in case of green-leaf phenology are related to phenological transition dates (Zhang et al., 2003). These extreme points are easily calculated as maximum and minimum points in the first and second derivatives of the double logistic function (Klostermann et al. (2014), and Fig. 2). We extracted the days (hereafter referred to as 'key dates') of (a) green-up [GU], (b) start-of-the-season [SoS], (c) maturity [Mat], (d) senescence [Sen], I end-of-the-season [EoS] and (f) dormancy [Dorm].

2.3. Sensitivity of parameter estimation

We accounted for uncertainties in our generated phenology, which could propagate into the estimation of key dates (Klostermann et al., 2014), by applying the so-called 'delta-method' (Butsic et al., 2010; Lewis et al., 2009). To do so, we calculated

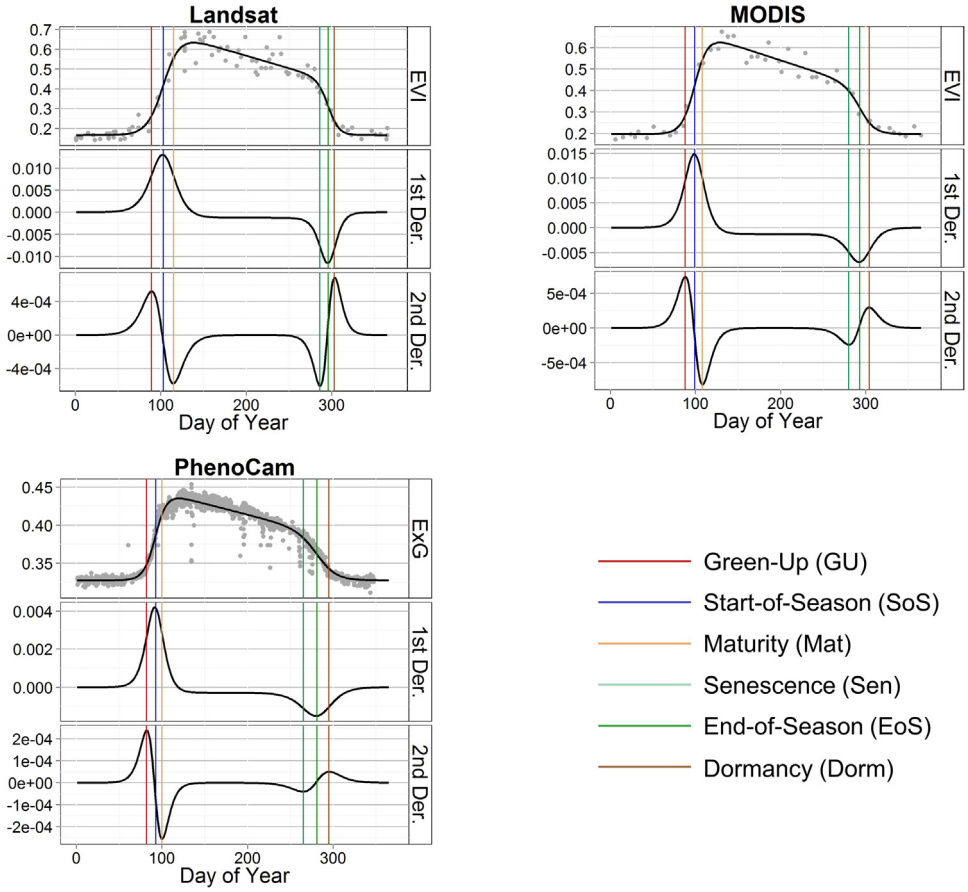

Fig. 2. Example of the three phenology-profiles (Landsat, PhenoCam and MODIS) and the estimation strategy of the key dates. The top row of each graph represents the EVI/E_xG_m time series; the middle and bottom row the first and second derivatives of the phenology profiles. The example represents the Mammoth Cave study site for the year 2012.

the parameter co-variance matrix from the output of the regression and estimated from it the 95% confidence intervals around the parameter estimates. We then randomly selected a set of parameter values from within these confidence intervals, fitted a phenology curve and subsequently estimated the key dates. We repeated this process 1000 times in a Monte-Carlo simulation and calculated the average and the standard deviation of the key dates, thus providing a measure of uncertainty.

2.4. Trend analysis of phenological key dates between 2002 and 2012

We applied our new methodology of (a) generating a dense Landsat time series and subsequently fitting a phenology curve, and (b) extracting key phenological dates to each year between 2002 and 2012, which resulted in a time series of phenological key dates from Landsat. We then assessed whether there were trends from 2002 to 2012 in these key dates (e.g., whether the SoS occurred earlier in later years). To do this we calculated the trend for each key date by calculating the Theil-Sen slope estimator (Sen, 1968). We chose this estimator over a simple linear regression because the Theil-Sen estimator is insensitive to outliers (Bagchi et al., 2007), which we were worried about given that had only 11 years of data. We estimated the Theil-Sen slope for each key date (i.e., GU, SoS, etc.) at each study site as well as the confidence intervals and significance levels.

2.5. Preparation of ground-based reference phenology

For validation, we selected PhenoCam data from stations for which data of an entire year was available (Table 1). PhenoCam data are true color digital photographs of the vegetation canopy and we pre-processed them in order to generate a phenological curve that could be compared to those from Landsat and MODIS. First, we downloaded all available pictures from the PhenoCam website. Second, we defined within each picture a region of interest that maximized the area of canopy that was included in all pictures, and excluded sky, understory, and forest floor (Richardson et al., 2009, 2007). Third, we extracted the digital values of all three channels (red, green and blue) of each digital picture and calculated the Excess Greeness Index ExG_M (Hufkens et al., 2012; Sonnentag et al., 2012):

$$\boldsymbol{ExG_m} = 2 \cdot \boldsymbol{G} - (\boldsymbol{R} - \boldsymbol{B}) \quad (2)$$

where *R, G, B* are the brightness levels of the green, red and blue channels. For this part of our analysis, we used the freely available MATLAB tool that is available on the PhenoCam-network website (http://phenocam.sr.unh.edu/webcam/). Once ExGM was estimated for each digital photograph, we applied Eq. (1) and the same parameter estimation strategy including the sensitivity analysis as for MODIS and Landsat to fit a phenology curve through the PhenoCam data, and extracted phenological key dates.

2.6. Comparison of the Landsat time series to MODIS and PhenoCam time series

To assess the validity of our new Landsat phenology, we compared the phenological key dates derived from Landsat and MODIS with those derived from the PhenoCam data, resulting in a sample size of 29 (Table 1). Specifically, we made three comparisons: (a) Landsat vs. MODIS, (b) Landsat vs. PhenoCam, and (c) MODIS vs. PhenoCam, and we evaluated each comparison in form of a scatter plot and by calculating Pearson's correlation coefficient as a measure of agreement. In case of comparison (a), we accounted for the variability of several Landsat pixels within one MODIS pixel, by estimating the key dates for all Landsat pixels that were entirely within one MODIS pixel, and by calculating their mean and standard deviation. For comparison (b) we additionally accounted for the wide field-of-view by the PhenoCam and therefore considered the Landsat pixel of the PhenoCam location and the three pixels in front of it (i.e., the pixel in front of the PhenoCam location plus the two pixels to the left and right of it). Again, we calculated the mean and standard deviation of the estimated key dates. Lastly, in case of comparison (c) we compared the key dates of the MODIS pixel to the key dates of the PhenoCam.

3. Results

By using multi-year imagery we were able to substantially sharpen the phenology curves for each individual year in each study region (Table 2). Prior to merging, the number of available cloud-free observations was low in many cases (5.2–12 images per year), making it impossible to fit a five-parameter phenology curve. After merging, we had on average 94.3 clear-sky observations in each time series (standard deviation of 8.8 images). Most observations were available at the Morgan Monroe State Forest (105.25 observations) and Mammoth Cave (102.1 observations) stations, the least at Arbutus Lake (75.6, Table 2). As a result, we were able to fit for each year between 2002 and 2012 at each location a phenology curve from Landsat.

The trend analysis suggested that the phenology at our study sites changed considerably from 2002 to 2012. These changes were particularly pronounced during the first part of the growing season, and our regression analyses suggest that GU, SoS, and Mat of vegetation occurred earlier in 2012 compared to 2002. The strongest trend occurred at the Harvard Forest site (SoS on average 1.9 days earlier per year, Mat 1.86 days earlier), whereas the Cary Institute site showed a later start of the season (on average 0.4, 0.2, 0.4 days later per year, Fig. 3). Surprisingly, the key dates during the second half of season also ended earlier at most of our study sites, but this trend was much less pronounced (Fig. 3, Table 4).

The estimated key dates showed strong similarities between MODIS and Landsat. We found on average a correlation coefficient of 0.882 (GU = 0.95, SoS = 0.94, Mat = 0.86, Sen = 0.85, EoS = 0.91 and Dorm = 0.79; Table 3, Fig. 4). The Landsat and the PhenoCam showed an average correlation coefficient of 0.85 (GU = 0.94, SoS = 0.93, Mat = 0.80, Sen = 0.80, EoS = 0.83 and Dorm = 0.81; Table 3). The weakest relationship occurred between MODIS and PhenoCam, and had an average of 0.79 (GU = 0. 85, SoS = 0.77, Mat = 0.74, Sen = 0.80, EoS = 0.78 and Dorm = 0.83; Table 3). In addition, the Monte-Carlo simulations suggest that the key date estimations were most robust when based on our new Landsat time series (average standard deviation of 4.6 days across all stations and years) compared to the MODIS estimations (21.6 days), and the Landsat based estimates were also much more similar to the PhenoCam estimations (3.0 days, Fig. 4).

In the Landsat vs. MODIS comparison, the difference between the key dates was higher during the first part of the growing season (GU = −7.9, −7.9, and −6.4 days) (Fig. 5), compared to the second part of the growing season, where the differences were within 2.7 days for Sen, EoS and Dorm (+0.9, +2.7, and +1.3 days, Fig. 6). All three key dates during the first part of the growing season (i.e., GU, SoS, and Mat) were estimated earlier by the PhenoCam. In the Landsat vs. PhenoCam comparison the differences were less pronounced (GU, SoS and Mat date differences of +4.4, +6.8, +12.2 days respectively) than for MODIS (+ 12.1, + 14.5, +18.1 days). However, during the second half of the growing season dates were closer (+1.6, +1.6, +2.9 days for Landsat vs. PhenoCam; 0.8, −1.1, +1.5 days for GU, SoS and Mat for MODIS vs. PhenoCam, Fig. 6).

4. Discussion

Remote sensing is a powerful tool to characterize phenology across large areas. Several ecological applications such as the estimation of annual evapotranspiration work well with MODIS derived phenology, available at 250–500-m spatial resolution. However, other applications such as the characterization of bird migration or the classification of mixed forests would benefit from phenological information at finer spatial resolutions, which for example Landsat imagery can provide (e.g., (Wolter et al., 1995; Wolter and Townsend 2011; Wood and Pidgeon 2015)). The challenge is that Landsat data are often too infrequent in a given year to estimate phenology accurately. Here, we present a new method that combines Landsat images of multiple years and MODIS data to generate phenology curves at Landsat's 30 m resolution for every year, and with higher robustness in their estimation. By combining multi-year imagery we were able to create a dense Landsat time series for 11 years that strongly corresponded to phenology estimates from ground-based validation data. Furthermore, we were able to identify trends in key phenological dates, which generally occurred earlier in later years.

Our results show that the combination of multi-year imagery can provide Landsat-based phenology curves for each year, which was not possible with the images recorded for any given year by itself. We tested our approach in footprints for which 75–100 images recorded over 11 years were available. We suggest though that our approach would also work with a lower number of years from which Landsat imagery are available. For example, taking only Landsat imagery in account from years for which we had PhenoCam data, the station Harvard Forest would have almost 40 clear-sky Landsat observations available (Table 2) to generate a phenology curve. Likewise, at Morgan Monroe State Park there are ~33 clear-sky observations available from only three years (Table 2). Thus, although not tested here, in data-rich regions a lower amount of years would likely suffice to create a phenology curve from Landsat. Conversely, for regions in which data is less available and cloud cover more prevalent compared, the currently archived scenes most likely will suffice to produce a phenology curve there as well when all years between 2002 and 2012 would be used. Thus, considering the current status of the Landsat Global Archive Consolidation (http://landsat.usgs.gov/documents/StateOfTheArchive_web.pdf) and the ongoing consolidation efforts, we suggest that our approach allows generating a phenology curve is applicable in most places where vegetation exhibits a clear phenological pattern throughout the year, emphasizing the value of our method for global phenology applications.

By using MODIS EVI time series and DTW to re-align Landsat imagery from multiple years we were able to generate a temporally dense time series of Landsat data. This confirms findings in a study region in Norway using a combination of MODIS and AVHRR NDVI time series (Huseby et al., 2005). However, Huseby et al. (2005) only used a handful of Landsat images, whereas we took advantage of all available Landsat images between 2002 and 2012,

Table 2
Number of clear-sky observations available at each study site and for each year that was analyzed. Clear-sky observation here refers to the location of the PhenoCam itself after the pre-processing of the Landsat images that involved the masking of clouds and cloud shadows using Fmask. The number of observations of all years reflects all Landsat observations available between 2002 and 2012. The average and standard deviation reflects the average of all Landsat pixels that fell within one MODIS pixel.

Station	Year	Average # of Observations	STD # of Observations
Arbutus Lake	2009	6.2	0.42
	2010	6.7	0.47
	2012	8	0
	2002–2012	75.7	1.24
Bartlett	2008	10	0
	2009	9.3	0.47
	2011	9	0
	2012	12	0
	2002–2012	96	1.05
Cary Institute	2010	10.42	0.49
	2012	11	0
	2002–2012	90.1	2.59
Harvard Forest	2009	10	0
	2010	10.125	0.93
	2011	9.5	0.5
	2012	9	0
	2002–2012	96.25	0.83
Morgan Monroe State Forest	2010	10.42	0.49
	2011	8.42	0.73
	2012	13	0
	2002–2012	105.25	0.66
Univ. Michigan Biological Station	2010	8.8	0.6
	2011	12.5	0.5
	2012	10	0
	2002–2012	95.1	1.81
Mammoth Cave	2003	12	0
	2004	9	0
	2005	8.7	0.63
	2006	12.55	0.83
	2007	5.2	0.79
	2008	10.7	0.42
	2009	5.3	0.47
	2011	9	0
	2012	8.3	0.67
	2002–2012	102.1	1.09

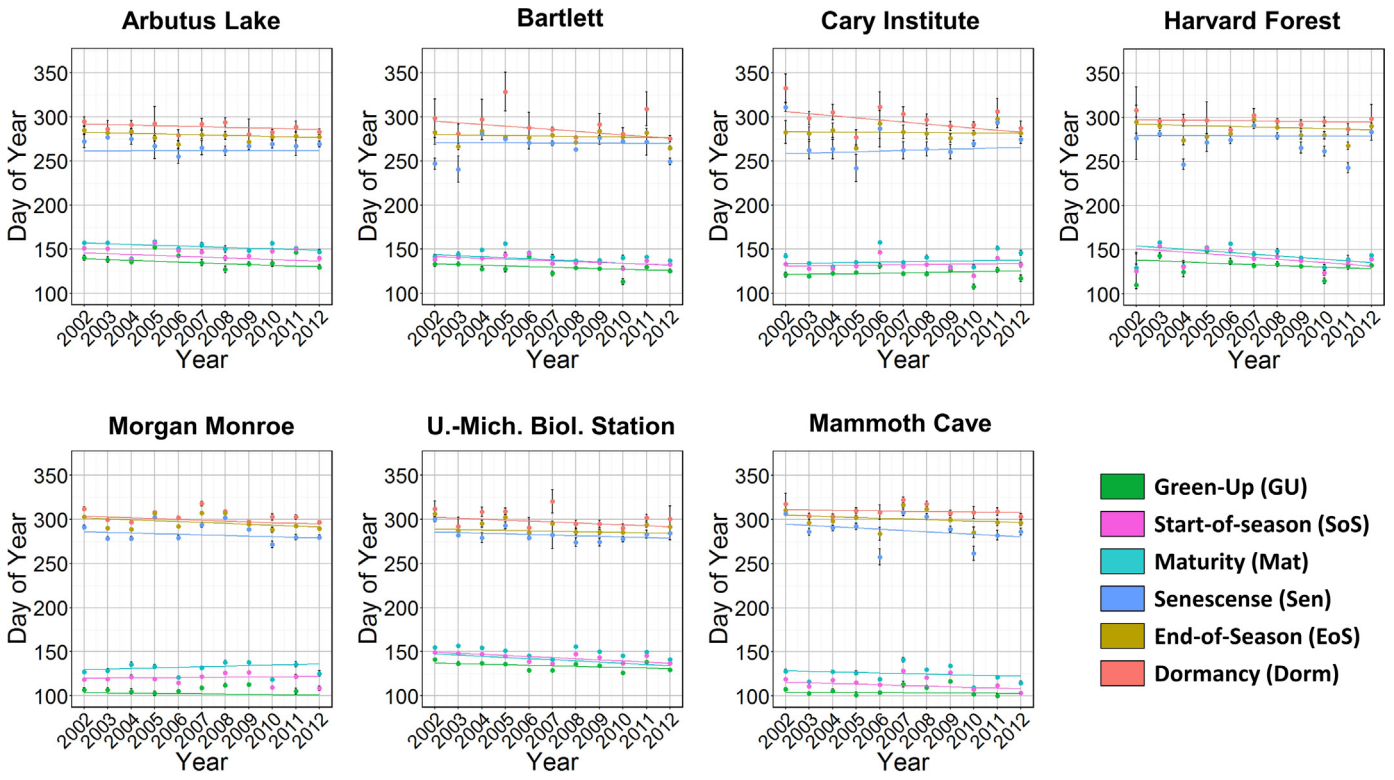

Fig. 3. Changes in phenological key dates between 2002 and 2012 as derived from the new Landsat phenology product. The points represent the estimates for each year, together with the standard deviations, which we derived from the Landsat pixels analyzed. The lines describe are the result of the linear regression and can be interpreted as the trend for each key date over the time period we analyzed.

Table 3
Mean values of the correlation coefficients for estimated key dates between the Landsat-MODIS and Landsat-PhenoCam comparisons after 1000 Monte-Carlo simulation runs. The values in brackets represent the standard deviation.

Comparison	Key date					
	Green-Up	Start-of-Season	Maturity	Senescence	End-of-Season	Dormancy
MODIS vs. PhenoCam	0.845 (0.165)	0.766 (0.192)	0.735 (0.196)	0.804 (0.189)	0.784 (0.154)	0.832 (0.181)
Landsat vs. MODIS	0.948 (0.116)	0.942 (0.132)	0.859 (0.182)	0.855 (0.174)	0.908 (0.089)	0.787 (0.232)
Landsat vs. PhenoCam	0.944 (0.125)	0.925 (0.135)	0.803 (0.166)	0.805 (0.192)	0.803 (0.166)	0.807 (0.209)

Table 4
Results from the trend analysis using the Theil-Sen slope estimator. Results are presented for each site and key date individually, including the standard error of the estimated slope ('upper limit' and 'lower limit') of the regression line.

Station	Key date	Slope estimate	Lower limit	Upper limit	V-Value	P(>|V|)
Arbutus Lake	GU	−0.935	−2.094	−0.396	8	0.024
	SoS	−0.955	−1.176	0.052	12	0.067
	Mat	−0.833	−1.023	0.415	12	0.067
	Sen	0.007	−0.974	0.464	28	0.700
	EoS	−0.597	−0.912	−0.127	10	0.042
	Dorm	−0.636	−1.020	−0.110	8	0.024
Bartlett	GU	−0.772	−1.781	−0.302	3	0.005
	SoS	−0.909	−1.384	−0.649	0	0.001
	Mat	−1.222	−1.542	−0.521	0	0.001
	Sen	−0.133	−1.449	1.894	26	0.577
	EoS	−0.319	−1.262	0.692	23	0.413
	Dorm	−1.951	−2.448	0.779	13	0.083
Cary Institute	GU	0.417	−1.133	0.577	33	1.000
	SoS	0.283	−0.766	0.532	32	0.966
	Mat	0.454	−0.781	1.424	42	0.465
	Sen	0.731	−1.761	3.338	46	0.278
	EoS	−0.165	−0.445	1.365	23	0.413
	Dorm	−2.323	−3.580	−0.244	10	0.042
Harvard Forest	GU	−0.997	−2.360	0.993	21	0.320
	SoS	−1.986	−2.566	0.270	15	0.123
	Mat	−1.865	−2.714	0.229	11	0.054
	Sen	−0.057	−2.727	0.888	25	0.520
	EoS	−0.643	−1.758	0.531	21	0.320
	Dorm	−0.292	−1.305	0.127	15	0.123
Morgan Monroe	GU	−0.262	−1.156	0.389	25	0.520
	SoS	0.199	−0.695	0.713	38	0.700
	Mat	0.655	−0.661	0.946	40	0.577
	Sen	−0.702	−1.988	0.105	12	0.067
	EoS	−1.019	−1.254	0.220	14	0.102
	Dorm	−0.910	−1.279	−0.024	9	0.032
Morgan Monroe State Forest	GU	−0.640	−1.173	−0.333	5	0.010
	SoS	−1.257	−1.393	−0.685	0	0.001
	Mat	−1.350	−1.522	−0.738	1	0.002
	Sen	−0.720	−1.881	−0.001	10	0.042
	EoS	−0.430	−1.498	−0.006	10	0.042
	Dorm	−1.084	−1.616	−0.104	9	0.032
Univ. Michigan Biol. Station	GU	−0.107	−1.314	0.635	25	0.520
	SoS	−0.767	−1.245	0.352	20	0.278
	Mat	−0.616	−1.188	0.494	20	0.278
	Sen	−1.416	−2.874	−0.057	10	0.042
	EoS	−0.839	−1.702	−0.091	9	0.032
	Dorm	−0.313	−0.980	0.160	15	0.123
Mammoth Cave	GU	−0.772	−1.781	−0.302	3	0.005
	SoS	−0.909	−1.384	−0.649	0	0.001
	Mat	−1.222	−1.542	−0.521	0	0.001
	Sen	−0.133	−1.449	1.894	26	0.577
	EoS	−0.319	−1.262	0.692	23	0.413
	Dorm	−1.951	−2.448	0.779	13	0.083

allowing us to create a very dense Landsat time series, and hence the phenology curves for each year over a 10-year time span. Our approach is thus an advanced application of previous work using Landsat data and DTW. The re-alignment of Landsat data presented here is also different from other re-aligning approach of Landsat data. Specifically, rather than calculating relative phenological differences by employing a relative-measure of 'days-left-in-season' (Isaacson et al., 2012) our approach estimates exact key phenological dates, thus ultimately allowing to assess long-term trends in phenology. Our approach is more similar to the adjustment by Fisher et al. (2006) who also re-aligned Landsat imagery based on a reference year. However, our approach does not rely on a high data availability of Landsat imagery for a given year and may thus be particularly suitable for data scarce regions. Likewise, our approach is different from the work of Melaas et al. (2013) because the fitting of an individual phenological curve for each year may not result in reasonable phenology curves when the number of Landsat observations is barely higher than the number of parameters in the phenology function.

In general, we found a stronger agreement between key dates extracted from Landsat and those from MODIS (i.e., the Landsat vs. MODIS comparison), than between Landsat and the PhenoCam

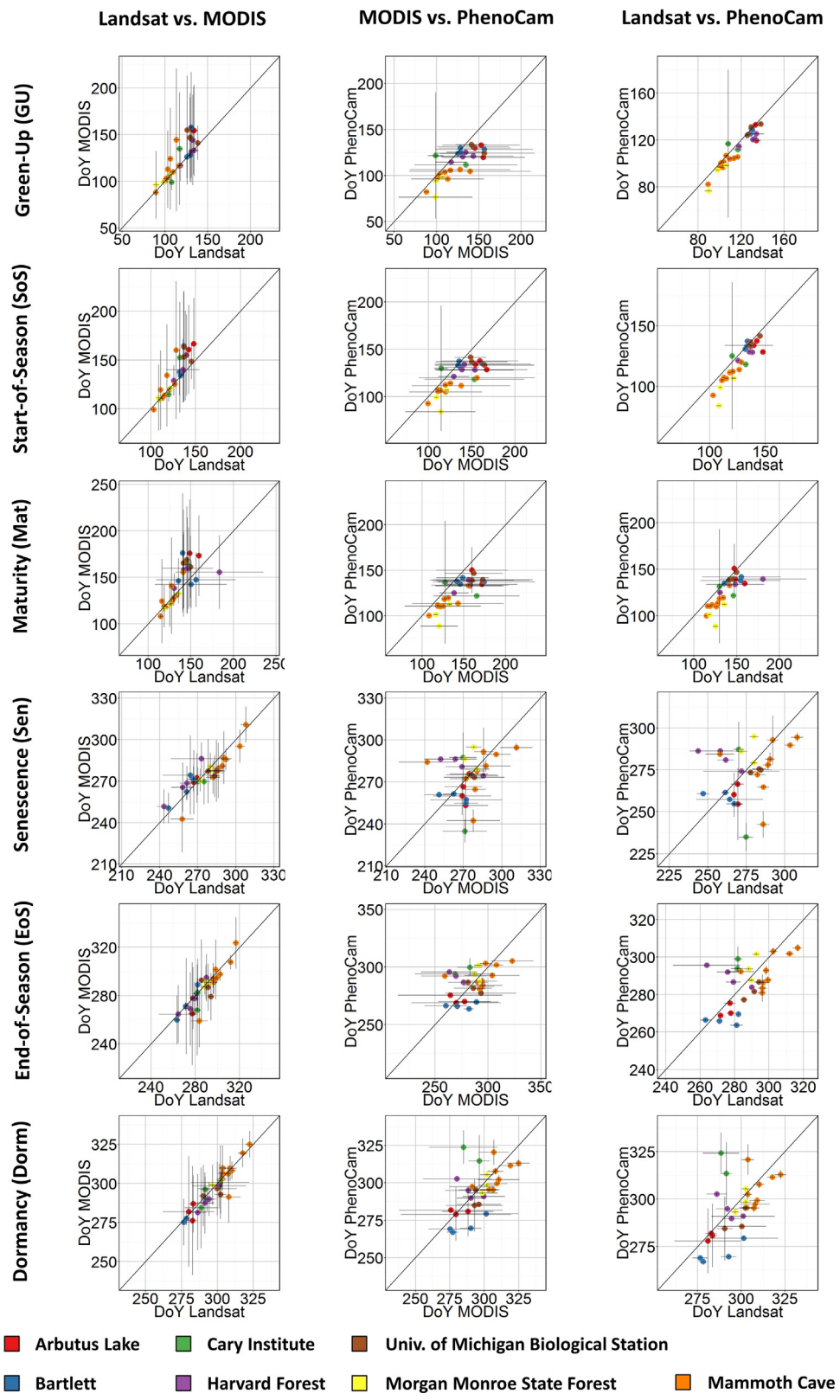

Fig. 4. Scatterplots of the estimated key dates of each of our three comparisons. The right column represents the Landsat vs. PhenoCam comparisons, the middle column the MODIS- vs. PhenoCam comparison, and left column the Landsat vs. MODIS comparisons. The different colors represent the different study areas and the number of points is determined by the number of reference years (Table 1). The point locations represent the mean estimated key dates of 1000 Monte-Carlo simulations, the error bars the calculated standard deviations.

(Landsat vs. PhenoCam) and this finding was consistent across all locations. This was expected, because we used MODIS data to re-align the Landsat observations. The Landsat-PhenoCam comparison was an independent comparison, and while agreement was generally strong, there were more pronounced differences. Several causes may have contributed to these differences. First, there are

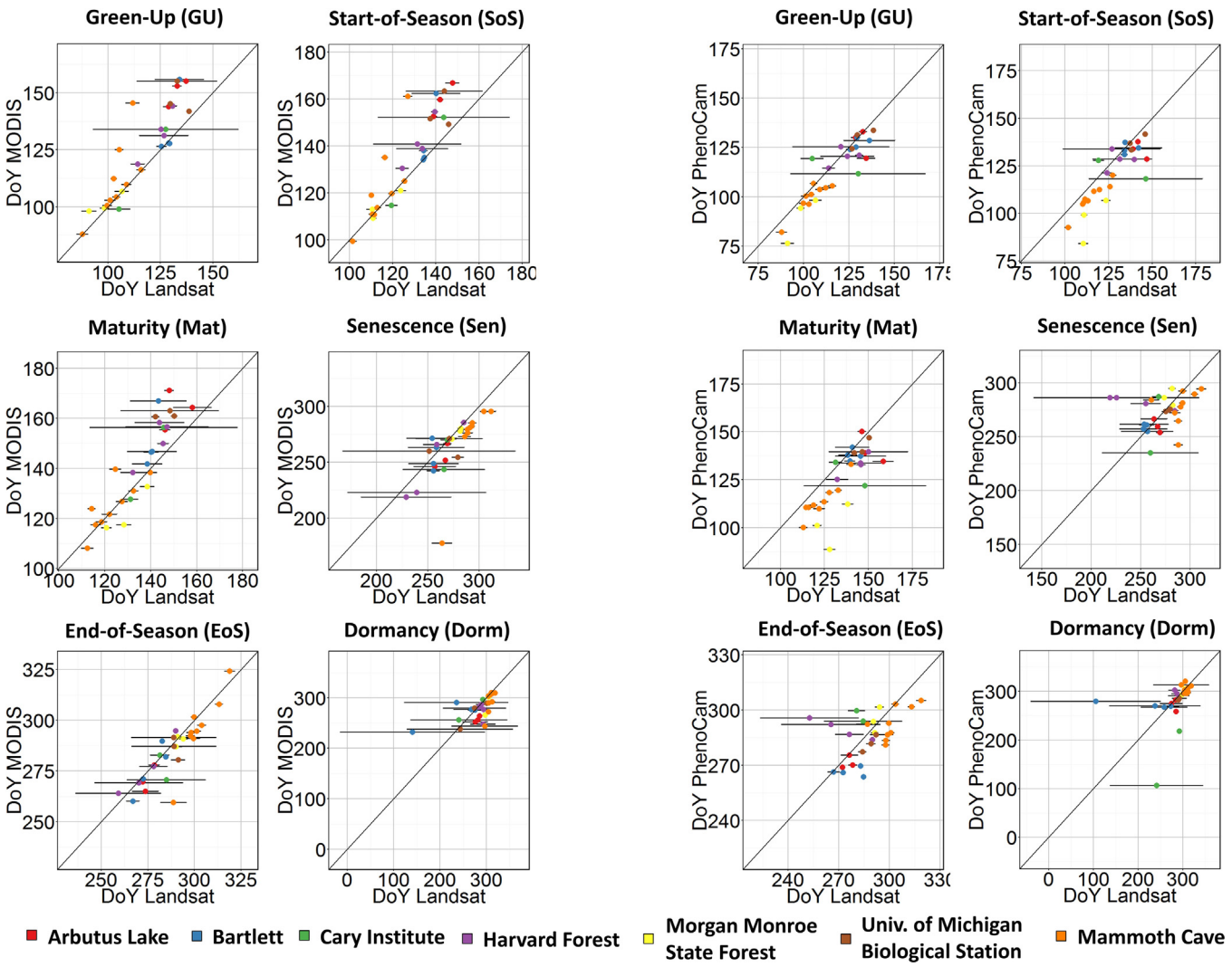

Fig. 5. Scatterplots exemplifying the variability in estimated key dates from all Landsat pixels within one MODIS pixel (left side), as well as the variability of all Landsat pixels in the field-of-view of a PhenoCam (right side). For presentation purposes the values here are only the mean estimates from 1000 Monte-Carlo simulations. The points indicate the mean values of the Landsat pixels (i.e., the mean key date of all Landsat pixels within the MODIS pixel; and the mean key date of all Landsat pixels in the field-of-view of the PhenoCam), the error bars the standard deviations of the estimates.

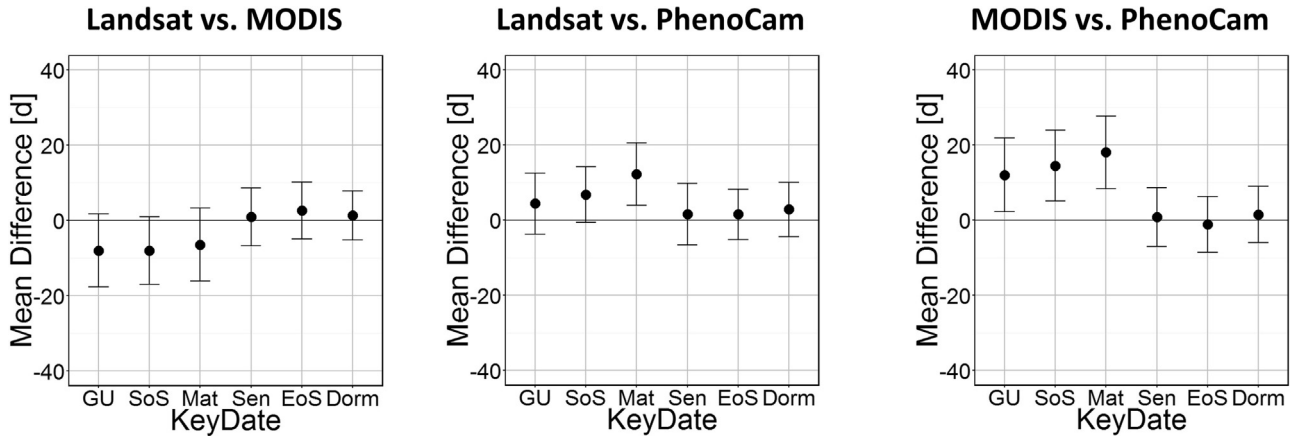

Fig. 6. Difference of estimated key dates for each of our three comparisons, Landsat vs. MODIS (left), Landsat vs. PhenoCam (center) and MODIS vs. PhenoCam (right). The values represent the mean difference in the key dates across all locations and reference years, the error bars are the standard deviation.

fundamental differences in the different data sets. Previous work suggests that the camera field of view (FOV) associated with the oblique look angle of digital pictures strongly affects the agreement between MODIS and PhenoCam at broad scales (Hufkens et al., 2012). At fine scales, spring onset of leaf area index (LAI) as well as morphological measures such as leaf size, often lag behind

spring onset measured from the PhenoCam (Keenan et al., 2014), likely affecting the comparison of phenological measurements from satellites with those from PhenoCam. Thus, we suggest that the observed differences between the phenologies (i.e., Landsat, MODIS and PhenoCam) in our study need to be interpreted with caution (Richardson et al., 2007).

At the same time, the agreement between Landsat and PhenoCam was higher than between MODIS and PhenoCam. We suggest that this is due to the higher spatial resolution of Landsat compared to MODIS and hence less spectral influence of neighboring (possibly non-forest) locations. Lastly, our Monte-Carlo simulations suggest that the error from the non-linear regressions was much smaller for Landsat compared to MODIS, most likely a result of the very high observation density. In summary, our new Landsat phenology is an improvement on two frontiers: first, our Landsat phenology provides phenological information with much higher spatial resolution than MODIS. Second, the higher agreement of our Landsat phenology with PhenoCam phenologies highlights the value of using ground-based point-location information of phenology to validate large-scale assessments from satellite data. Lastly, the high observation density in our Landsat time series provides much more robust estimates of key dates than would be possible from the Landsat record for a single year alone.

Our results also indicated that all key dates extracted from PhenoCam occurred earlier than in Landsat. We are not entirely sure what may have caused this because we anticipated Landsat to be more sensitive to understory green-up, which almost always occurs earlier than the overstory green-up in temperate forests (Augspurger and Bartlett, 2003). PhenoCam cameras, with their oblique view and the selected analysis mask, focus generally on overstory vegetation rather than the understory. However, Landsat observations have nadir view and as such would be expected to be more sensitive to understory vegetation. Especially during the first half of the growing season, the key dates from Landsat should thus be earlier than those from PhenoCam, but our results suggest the opposite. Nevertheless, while not neglecting these observational differences between Landsat and PhenoCam datasets, we note that the primary goal of this study was to create a phenology product from Landsat that was comparable to that of MODIS, but at much finer resolution, and we certainly succeeded in this. Furthermore, our results suggest that from 2002 to 2012 there was a trend towards an earlier start of the growing season. The reasons for that may be milder winters or earlier spring onsets, as especially the GU and SoS dates are directly linked to temperature (Badeck et al., 2004).

Despite the overall promising results, some uncertainties are worth mentioning. First, we did not test how changes in land cover that change EVI values substantially, for example a clear-cut harvest, would affect our results. Likewise, our study was limited to forested landscapes and did not include agricultural areas, making it uncertain how the approach would perform in these cases. The reason why we did not investigate agricultural areas was that our goal was to develop the new methodology, and provide a proof of concept. Applying our methods in different land-cover types, or in mixed pixels was beyond the scope of our work. Second, our approach requires information about yearly 'reference' phenologies from other data sources. Here, we used MODIS data, but data from other sensors such as AVHRR could potentially yield similar results and would allow analyzing pre-2002 Landsat imagery as well. This would need to be tested carefully though. Third, although we tested for the variation of Landsat pixels within the reference MODIS pixel, some uncertainties may remain from combining MODIS EVI products from Aqua and Terra within one time series. However, we consider these marginal. Lastly, the trend analysis is based on a rather short time series (i.e., 11 years) and as such it is hard to estimate the long term trend of phenological key dates.

Green-leaf phenology is an important ecological measure that describes the vegetation dynamics throughout a year, and remote sensing is a powerful tool to describe green-leaf phenology at broad scales. MODIS data have been used to routinely generate phenology data, but finer-resolution phenology data from Landsat satellite imagery have been missing because of limited data availability in individual years. Here, we present a new approach that allows characterizing phenology from Landsat data across larger time periods even when the number of clear-sky observations is low. Our results showed that there is strong agreement between the resulting Landsat phenology and the MODIS phenology, and good agreement with phenology observed on the ground from PhenoCam. This suggests that our green-leaf phenology from Landsat has the potential to be valuable for applications that require understanding the processes that shape the Earth's surface at fine spatial resolution. For example, one application may be the mapping of forest composition in mixed stands with satellite imagery (Wolter and Townsend, 2011) or the distribution of aspen-clones in the landscape (Li et al., 2010). Other ecological applications such as characterization of bird migrations based on the phenological state of vegetation (Wood and Pidgeon 2015; Wood et al., 2012) or habitat selection by red deer (Schaefer et al., 2008) could also benefit from a Landsat phenology product, because the continuous measure introduced here capture the state of the vegetation at a spatial resolution that is close to the way animals perceive landscapes. To this end, the Landsat phenology method and the derived products described here could become a valuable tool to improve the understanding of the interaction between the biosphere and climate.

Acknowledgements

We thank E. Wood, M. Friedl, P. Griffiths, P. Townsend, D. Pflugmacher, and S. Carter for valuable discussions and comments on earlier versions of the manuscript. This research was funded by the Land-Cover/Land-Use Change (LCLUC) program of the National Aeronautics and Space Administration (NASA) through grant NNX08AK77G, and by a UW-Madison McIntire-Stennis Formula Program grant (WIS01715). ADR acknowledges support from the Northeastern States Research Cooperative, NSF's Macrosystems Biology program (award EF-1065029), the US National Park Service Inventory and Monitoring Program and the USA National Phenology Network (grant number G10AP00129 from the United States Geological Survey).

References

Asner, G.P., Townsend, A.R., Braswell, B.H., 2000. Satellite observation of El Nino effects on Amazon forest phenology and productivity. Geophys. Res. Lett. 27, 981–984.

Augspurger, C.K., Bartlett, E.A., 2003. Differences in leaf phenology between juvenile and adult trees in a temperate deciduous forest. Tree Physiol. 23, 517–525.

Badeck, F.-W., Bondeau, A., Böttcher, K., Doktor, D., Lucht, W., Schaber, J., Sitch, S., 2004. Responses of spring phenology to climate change. New Phytol. 162, 295–309.

Bagchi, A., Chaudhary, A., Eppstein, D., Goodrich, M.T., 2007. Deterministic sampling and range counting in geometric data streams. ACM Trans. Algorithms 3, 16.

Bhandari, S., Phinn, S., Gill, T., 2012. Preparing landsat image time series (LITS) for monitoring changes in vegetation phenology in Queensland, Australia. Remote Sens. 4, 1856–1886.

Butsic, V., Lewis, D.J., Radeloff, V.C., 2010. Lakeshore zoning has heterogeneous ecological effects: an application of a coupled economic-ecological model. Ecol. Appl. 20, 867–879.

Crawley, M.J., Akhteruzzaman, M., 1988. Individual variation in the phenology of oak trees and its consequences for herbivorous insects. Funct. Ecol. 2, 409–415.

Elmore, A.J., Guinn, S.M., Minsley, B.J., Richardson, A.D., 2012. Landscape controls on the timing of spring, autumn: and growing season length in mid-Atlantic forests. Global Change Biol. 18, 656–674.

Fisher, J.I., Mustard, J.F., Vadeboncoeur, M.A., 2006. Green leaf phenology at Landsat resolution: scaling from the field to the satellite. Remote Sens. Environ. 100, 265–279.

Ganguly, S., Friedl, M.A., Tan, B., Zhang, X.Y., Verma, M., 2010. Land surface phenology from MODIS: characterization of the collection 5 global land cover dynamics product. Remote Sens. Environ. 114, 1805–1816.
Gao, F., Masek, J., Schwaller, M., Hall, F., 2006. On the blending of the Landsat and MODIS surface reflectance: predicting daily Landsat surface reflectance. IEEE Trans. Geosci. Remote Sens. 44, 2207–2218.
Giorgino, T., 2009. Computing and visualizing dynamic time warping alignments in R: the dtw package. J. Stat. Softw. 31, 1–24.
Goward, S.N., Tucker, C.J., Dye, D.G., 1985. North-American vegetation patterns observed with the Noaa-7 advanced very high-resolution radiometer. Vegetatio 64, 3–14.
Hall, D., Luquez, V., Garcia, V.M., St Onge, K.R., Jansson, S., Ingvarsson, P.K., 2007. Adaptive population differentiation in phenology across a latitudinal gradient in European Aspen (*Populus tremula*, L.): a comparison of neutral markers, candidate genes and phenotypic traits. Evolution 61, 2849–2860.
Hilker, T., Wulder, M.A., Coops, N.C., Seitz, N., White, J.C., Gao, F., Masek, J.G., Stenhouse, G., 2009. Generation of dense time series synthetic Landsat data through data blending with MODIS using a spatial and temporal adaptive reflectance fusion model. Remote Sens. Environ. 113, 1988–1999.
Hufkens, K., Friedl, M., Sonnentag, O., Braswell, B.H., Milliman, T., Richardson, A.D., 2012. Linking near-surface and satellite remote sensing measurements of deciduous broadleaf forest phenology. Remote Sens. Environ. 117, 307–321.
Huseby, R.B., Aurdal, L., Eikvil, L., Solberg, R., Vikhamar, D., Solberg, A., 2005. Alignment of growth seasons from satellite data. 2005 International Workshop on the Analysis of Multi-Temporal Remote Sensing Images (IEEE Cat. No. 05EX1064), 213–216.
Isaacson, B., Serbin, S., Townsend, P., 2012. Detection of relative differences in phenology of forest species using Landsat and MODIS. Landscape Ecol. 27, 529–543.
Keenan, T.F., Darby, B., Felts, E., Sonnentag, O., Friedl, M.A., Hufkens, K., O'Keefe, J., Klosterman, S., Munger, J.W., Toomey, M., Richardson, A.D., 2014. Tracking forest phenology and seasonal physiology using digital repeat photography: a critical assessment. Ecol. Appl. 24, 1478–1489.
Klostermann, S.T., Hufkens, K., Gray, J.M., Melaas, E.K., Sonnentag, O., Lavine, I., Mitchell, L., Norman, R., Friedl, M.A., Richardson, A.D., 2014. Evaluating remote sensing of deciduous forest phenology at multiple spatial scales using PhenoCam imagery. Biogeosci. Discuss. 11, 2305–2342.
Knudby, A., 2004. An AVHRR-based model of groundnut yields in the peanut basin of senegal. Int. J. Remote Sens. 25, 3161–3175.
Kovalskyy, V., Roy, D.P., Zhang, X.Y., Ju, J., 2011. The suitability of multi-temporal web-enabled Landsat data NDVI for phenological monitoring – a comparison with flux tower and MODIS NDVI. Remote Sens. Lett. 3, 325–334.
Lechowicz, M.J., 1984. Why do temperate decidious trees leaf out at different times – adaptation and ecology of forest communities. Am. Nat. 124, 821–842.
Lewis, D.J., Provencher, B., Butsic, V., 2009. The dynamic effects of open-space conservation policies on residential development density. J. Environ. Econ. Manage. 57, 239–252.
Li, H., Wang, X., Hamann, A., 2010. Genetic adaptation of aspen (*Populus tremuloides*) populations to spring risk environments: a novel remote sensing approach. Can. J. For. Res. 40, 2082–2090.
Loveland, T.R., Dwyer, J.L., 2012. Landsat: building a strong future. Remote Sens. Environ. 122, 22–29.
Luquez, V., Hall, D., Albrectsen, B.R., Karlsson, J., Ingvarsson, P., Jansson, S., 2008. Natural phenological variation in aspen (*Populus tremula*): the SwAsp collection. Tree Genet. Genomes 4, 279–292.
Masek, J.G., Vermote, E.F., Saleous, N.E., Wolfe, R., Hall, F.G., Huemmrich, K.F., Feng, G., Kutler, J., Teng-Kui, L., 2006. A landsat surface reflectance dataset for North America, 1990–2000. Geosci. Remote Sens. Lett. IEEE 3, 68–72.
Melaas, E.K., Friedl, M.A., Zhu, Z., 2013. Detecting interannual variation in deciduous broadleaf forest phenology using Landsat TM/ETM+ data. Remote Sens. Environ. 132, 176–185.
Moré, J., 1978. The Levenberg-Marquardt algorithm: implementation and theory. In: Watson, G.A. (Ed.), Numerical Analysis. Springer, Berlin, Heidelberg, pp. 105–116.
Paruelo, J.M., Epstein, H.E., Lauenroth, W.K., Burke, I.C., 1997. ANPP estimates from NDVI for the central grassland region of the United States. Ecology 78, 953–958.
Petitjean, F., Ketterlin, A., Gancarski, P., 2011. A global averaging method for dynamic time warping: with applications to clustering. Pattern Recogn. 44, 678–693.
Petitjean, F., Inglada, J., Gancarski, P., 2012. Satellite image time series analysis under time warping. IEEE Trans. Geosci. Remote Sens. 50, 3081–3095.
Richardson, A.D., Bailey, A.S., Denny, E.G., Martin, C.W., O'Keefe, J., 2006. Phenology of a northern hardwood forest canopy. Global Change Biol. 12, 1174–1188.
Richardson, A.D., Jenkins, J.P., Braswell, B.H., Hollinger, D.Y., Ollinger, S.V., Smith, M.L., 2007. Use of digital webcam images to track spring green-up in a deciduous broadleaf forest. Oecologia 152, 323–334.
Richardson, A.D., Braswell, B.H., Hollinger, D.Y., Jenkins, J.P., Ollinger, S.V., 2009. Near-surface remote sensing of spatial and temporal variation in canopy phenology. Ecol. Appl. 19, 1417–1428.
Richardson, A.D., Keenan, T.F., Migliavacca, M., Sonnentag, O., Ryu, Y., Toomey, M., 2013. Climate change, phenology, and phenological control of vegetation feedbacks to the climate system. Agric. For. Meteorol. 169, 156–173.
Roetzer, T., Wittenzeller, M., Haeckel, H., Nekovar, J., 2000. Phenology in central Europe – differences and trends of spring phenophases in urban and rural areas. Int. J. Biometeorol. 44, 60–66.
Romani, L.A.S., Goncalves, R.R.V., Zullo, J., Traina Jr., C., Traina, A.J.M., 2010. New DTW-based method to similarity search in sugar cane regions represented by climate and remote sensing time series. In: Geoscience and Remote Sensing Symposium (IGARSS), 2010 IEEE International, pp. 355–358.
Sakoe, H., Chiba, S., 1978. Dynamic-programming algorithm optimization for spoken word recognition. IEEE Trans. Geosci. Remote Sens. 26, 43–49.
Santos, M.J., Rosalino, L.M., Quinn, J., Loureiro, C.F., Santos-Reis, M., Ustin, S.L., 2014. Spatial and temporal variability in habitat use: badgers (*Meles meles* and *Taxidea taxus*) in Mediterranean ecosystems. In: EARSeL LUCC and NASA LCLUC Joint Workshop, March 17–18 2014. Berlin (Germany).
Schaefer, J.A., Morellet, N., Pepin, D., Verheyden, H., 2008. The spatial scale of habitat selection by red deer. Can. J. Zool. 86, 1337–1345.
Schriever, J.R., Congalton, R.G., 1995. Evaluating seasonal variability as an aid to cover-type mapping from Landsat Thematic Mapper in the Northeast. Photogramm. Eng. Remote Sens. 61, 321–327.
Sen, P.K., 1968. Estimates of the regression coefficient based on Kendall's tau. J. Am. Stat. Assoc. 63, 1379–1389.
Sonnentag, O., Hufkens, K., Teshera-Sterne, C., Young, A.M., Friedl, M., Braswell, B.H., Milliman, T., O'Keefe, J., Richardson, A.D., 2012. Digital repeat photography for phenological research in forest ecosystems. Agric. For. Meteorol. 152, 159–177.
Sun, R., Gao, X., Liu, C.M., Li, X.W., 2004. Evapotranspiration estimation in the Yellow River Basin: China using integrated NDVI data. Int. J. Remote Sens. 25, 2523–2534.
Tucker, C.J., Fung, I.Y., Keeling, C.D., Gammon, R.H., 1986. Relationship between atmospheric CO_2 variations and a satellite-derived vegetation index. Nature 319, 195–199.
Tucker, C.J., 1979. Red and photographic infrared linear combinations for monitoring vegetation. Remote Sens. Environ. 8, 127–150.
Walker, J.J., de Beurs, K.M., Wynne, R.H., Gao, F., 2012. Evaluation of Landsat and MODIS data fusion products for analysis of dryland forest phenology. Remote Sens. Environ. 117, 381–393.
Walker, J.J., de Beurs, K.M., Wynne, R.H., 2014. Dryland vegetation phenology across an elevation gradient in Arizona, USA: investigated with fused MODIS and Landsat data. Remote Sens. Environ. 144, 85–97.
Weber, J., Petitjean, F., Gancarski, P., 2012. Towards efficient satellite image time series analysis: combination of dynamic time warping and quasi-flat zones. In: Geoscience and Remote Sensing Symposium (IGARSS), 2012 IEEE International, pp. 4387–4390.
Wolfe, D.W., Schwartz, M.D., Lakso, A.N., Otsuki, Y., Pool, R.M., Shaulis, N.J., 2005. Climate change and shifts in spring phenology of three horticultural woody perennials in northeastern USA. Int. J. Biometeorol. 49, 303–309.
Wolter, P.T., Townsend, P.A., 2011. Multi-sensor data fusion for estimating forest species composition and abundance in northern Minnesota. Remote Sens. Environ. 115, 671–691.
Wolter, P.T., Mladenoff, D.J., Host, G.E., Crow, T.R., 1995. Improved forest classification in the northern lake-states using multitemporal landsat imagery. Photogramm. Eng. Remote Sens. 61, 1129–1143.
Wood, E.M., Pidgeon, A.M., 2015. Extreme variations in spring temperature affect ecosystem regulating services provided by birds during migration. Ecosphere 6, art216.
Wood, E.M., Pidgeon, A.M., Liu, F., Mladenoff, D.J., 2012. Birds see the trees inside the forest: the potential impacts of changes in forest composition on songbirds during spring migration. For. Ecol. Manage. 280, 176–186.
Wulder, M.A., Masek, J.G., Cohen, W.B., Loveland, T.R., Woodcock, C.E., 2012. Opening the archive: how free data has enabled the science and monitoring promise of Landsat. Remote Sens. Environ. 122, 2–10.
Yan, L., Roy, D.P., 2014. Automated crop field extraction from multi-temporal web enabled landsat data. Remote Sens. Environ. 144, 42–64.
Zhang, X.Y., Friedl, M.A., Schaaf, C.B., Strahler, A.H., Hodges, J.C.F., Gao, F., Reed, B.C., Huete, A., 2003. Monitoring vegetation phenology using MODIS. Remote Sens. Environ. 84, 471–475.
Zhang, X.Y., Friedl, M.A., Schaaf, C.B., 2006. Global vegetation phenology from Moderate Resolution Imaging Spectroradiometer (MODIS): evaluation of global patterns and comparison with in situ measurements. J. Geophys. Res. Biogeosci. 111.
Zhu, Z., Woodcock, C.E., 2012. Object-based cloud and cloud shadow detection in Landsat imagery. Remote Sens. Environ. 118, 83–94.